The Journal of Chemical Physics

Extended magnesium and calcium force field parameters for accurate ion–nucleic acid interactions in biomolecular simulations

Cite as: J. Chem. Phys. **154**, 171102 (2021); https://doi.org/10.1063/5.0048113
Submitted: 19 February 2021 • Accepted: 14 April 2021 • Published Online: 03 May 2021

Sergio Cruz-León, Kara K. Grotz and Nadine Schwierz

The Journal of Chemical Physics COMMUNICATION scitation.org/journal/jcp

Extended magnesium and calcium force field parameters for accurate ion–nucleic acid interactions in biomolecular simulations

Cite as: J. Chem. Phys. 154, 171102 (2021); doi: 10.1063/5.0048113
Submitted: 19 February 2021 • Accepted: 14 April 2021 •
Published Online: 3 May 2021

Sergio Cruz-León, Kara K. Grotz, and Nadine Schwierz[a)]

AFFILIATIONS

Department of Theoretical Biophysics, Max Planck Institute of Biophysics, Max-von-Laue-Str. 3, 60438 Frankfurt am Main, Germany

[a)]Author to whom correspondence should be addressed: nadine.schwierz@biophys.mpg.de

ABSTRACT

Magnesium and calcium play an essential role in the folding and function of nucleic acids. To correctly describe their interactions with DNA and RNA in biomolecular simulations, an accurate parameterization is crucial. In most cases, the ion parameters are optimized based on a set of experimental solution properties such as solvation free energies, radial distribution functions, water exchange rates, and activity coefficient derivatives. However, the transferability of such bulk-optimized ion parameters to quantitatively describe biomolecular systems is limited. Here, we extend the applicability of our previous bulk-optimized parameters by including experimental binding affinities toward the phosphate oxygen on nucleic acids. In particular, we systematically adjust the combination rules that are an integral part of the pairwise interaction potentials of classical force fields. This allows us to quantitatively describe specific ion binding to nucleic acids without changing the solution properties in the most simple and efficient way. We show the advancement of the optimized Lorentz combination rule for two representative nucleic acid systems. For double-stranded DNA, the optimized combination rule for Ca^{2+} significantly improves the agreement with experiments, while the standard combination rule leads to unrealistically distorted DNA structures. For the *add* A-riboswitch, the optimized combination rule for Mg^{2+} improves the structure of two specifically bound Mg^{2+} ions as judged by the experimental distance to the binding site. Including experimental binding affinities toward specific ion binding sites on biomolecules, therefore, provides a promising perspective to develop a more accurate description of metal cations for biomolecular simulations.

I. INTRODUCTION

Divalent metal cations play a vital role in a large variety of physiological processes. The specific requirement for metal cations, in particular, Ca^{2+} and Mg^{2+}, is especially pronounced in nucleic acid systems in which they stabilize the tertiary structure, drive folding, or catalyze chemical reactions.[1–8]

To capture the role of metal cations in folding and in function, all-atom molecular dynamics simulations are particularly suited to characterize the behavior of the ions and to provide a unique atomistic description of the dynamics. However, the accuracy of the simulations depends on the quality of the empirical force fields. In most cases, the ions are modeled as point charges and the electrostatic, dispersion, and excluded volume interactions are taken into account by a pairwise interaction potential. Specifically, the pair potential between particles i and j is modeled as the sum of the Coulomb and the 12-6 Lennard-Jones (LJ) potential,

$$V(r_{ij}) = \frac{q_i q_j}{4\pi\epsilon_0 r_{ij}} + 4\varepsilon_{ij}\left[\left(\frac{\sigma_{ij}}{r_{ij}}\right)^{12} - \left(\frac{\sigma_{ij}}{r_{ij}}\right)^{6}\right], \quad (1)$$

where q_i is the charge of atom i and r_{ij} is the distance between the particles. While the Coulomb term does not contain any adjustable parameters, the LJ diameter σ_{ij} and the interaction strength ε_{ij} are free to be optimized. Typically, the two parameters are optimized

to reproduce certain experimental properties in combination with a selected water model. Out of the multitude of physical properties, the solvation free energy, comprising the energy and entropy of ion hydration, is considered the most important thermodynamic property in the development of accurate ionic force fields.[9–14] In addition, the distance to the water oxygens, which contains important information on the structure of the first hydration shell, is frequently used.[9–12] Moreover, including kinetic properties in the parameterization such as water exchange rates has proven useful to reproduce dynamical processes such as cation binding and exchange.[15,16] In addition, successful parameterization strategies attempt to balance ion–water and ion–ion interactions by including experimental data for activity coefficient derivatives in the optimization[14,17–19] since single-ion properties are insufficient to reproduce thermodynamic and structural properties at finite salt concentrations. Using a balanced set of solution properties yields force fields that correctly describe ion–water and ion–ion interactions[12] and resolve the subtle differences between distinct metal cations and their specific binding affinities[20] or their influence on the water structure at interfaces.[21]

Since the parameters are optimized based on bulk properties, the question arises whether they can be transferred to simulate the interactions of ions with biomolecules. In some cases, force field parameters for similar functional groups can be transferred without further optimization. However, the transferability of ion parameters optimized based on bulk properties to biomolecular systems is limited[13,22] since the interactions between ions and functional groups on biomolecules are different from their interactions with water.

The aim of our current work is to extend the applicability of our previous bulk-optimized parameters[12] to quantitatively describe the interactions of Ca^{2+} and Mg^{2+} with nucleic acids. Hereby, we focus on the most important ion binding site on nucleic acids, namely, the non-bridging phosphate oxygen.[23–25] Targeting the ion–nucleic acid interactions while leaving the ion–water and ion–ion interactions unchanged seems to be the natural strategy since the latter are not affected by the presence of a biomolecule. In particular, a similar approach has been applied successfully by Panteva and co-workers[13] to optimize the charge-induced ion–RNA interactions of 12-6-4 potentials for Mg^{2+}, Mn^{2+}, Zn^{2+}, and Cd^{2+} based on experimental site-specific binding free energies derived from potentiometric pH titration data.[23]

By contrast, our current approach does not introduce additional terms in the interaction potential. Instead, we focus the optimization on the combination rules, which are an integral part of classical force fields, and empirically describe the interactions between dissimilar particles. The systematic adjustment of the combination rules offers a simple and efficient approach to simultaneously reproduce bulk solution properties and site-specific ion–nucleic acid interactions for the most commonly used 12-6 potentials.

In particular, following the work by Fyta and Netz[14] and previous similar studies,[18,26,27] we introduce scaling factors $\lambda_{\sigma,\varepsilon}$ in the Lorentz–Berthelot combination rules,

$$\sigma_{iR} = \frac{\lambda_\sigma^{iR}}{2}(\sigma_{ii} + \sigma_{RR}),\ \varepsilon_{iR} = \lambda_\varepsilon^{iR}\sqrt{\varepsilon_{ii}\varepsilon_{RR}}. \tag{2}$$

Here, R corresponds to the phosphate oxygen and i corresponds to the Mg^{2+} or Ca^{2+} ion. The Lorentz rule[28] yields the effective radius as the average of the radii of phosphate oxygen and the ion for which the Pauli repulsion becomes significant. Strictly speaking, the unmodified combination rule ($\lambda_\sigma^{iR} = 1$) is correct only in the limit of hard spheres, while the modification ($\lambda_\sigma^{iR} \neq 1$) allows us to take deviations into account. Similarly, the Berthelot rule[29] yields the induced dipole interaction strength between phosphate oxygen and the respective ion. In both cases, deviations from the unmodified rule ($\lambda_{\sigma,\varepsilon}^{iR} \neq 1$) can arise due to charge-induced dipole interactions or charge transfer, which render the interaction more attractive. Therefore, both combination rules can be used to take some of the polarization effects into account implicitly.

An alternative approach to take polarization effects into account is to use charge scaling.[30,31] However, since charge scaling modifies the interaction between all components, the bulk solution properties are no longer reproduced.

In the following, we discuss the optimization procedure and demonstrate the performance of the optimized Lorentz combination rule for double-stranded DNA and the *add* A-riboswitch by comparison to the experimental results from x-ray crystallography.

II. METHODS

A. Optimization procedure

The force field parameters for Mg^{2+} and Ca^{2+} from our previous work[12] in combination with the TIP3P water model[36] were used as a starting point (Table I). The parameters were previously optimized based on a balanced set of solution properties and designed to accurately reproduce the experimental solvation free energy, the activity derivative, and the characteristics of water exchange from the first hydration shell.[12] Similar to previous work,[13] we optimize the ion–nucleic acid interactions by calculating the ion binding affinity toward the phosphate oxygen of a dinucleotide. Using a grid search in the λ_σ^{iR} parameter space and alchemical transformations, we select the value of the scaling factor that reproduces the experimental binding affinity to the phosphate oxygen of dimethyl-phosphate (Table II).

Here, we mainly focus on the Lorentz rule since the adjustment of the Berthelot rule failed in previous work to reproduce experimental activity coefficient derivatives in electrolyte solutions.[14] Our results show that small changes in λ_σ^{iR} are sufficient to reproduce the experimental values, while no changes in λ_ε^{iR} were required. In addition, we explore the possibility to modify the Berthelot combination

TABLE I. Optimized force field parameters and scaling factors for Mg^{2+}, Ca^{2+}, and Cl^-. Note that the scaling factors are only valid in combination with the Cl^- parameters from Ref. 12 and the Amber force fields parmbsc0 + χ_{OL3}[32–34] or parmbsc1[35] for RNA and DNA.

Ion	σ_{ii}[a] (nm)	ε_{ii}[a] (kJ/mol)	Charge[a] (e)	$\lambda_\sigma^{i\mathrm{Cl}}$ [a]	λ_σ^{iR*} [b]
Mg^{2+}	0.162	0.604	+2	1.65	1.085
Ca^{2+}	0.226	2.338	+2	1.00	1.027
Cl^-	0.441	0.284	−1	1.00	1.00

[a]Parameters taken from Ref. 12.
[b]Current work.

TABLE II. Binding affinities ΔG_b^i and equilibrium ion–phosphate oxygen distances R_b for the optimized combination rules for Mg^{2+} and Ca^{2+} and from experiments.

	ΔG_b^i (k_BT)		R_b (Å)	
Ion	Current work	Expt.	Current work	Expt.
Mg^{2+}	−1.220 ± 0.40	−1.036[a]	2.03 ± 0.05	2.06[b]
Ca^{2+}	−0.919 ± 0.40	−0.921[a]	2.32 ± 0.08	2.32[c]

[a]Experimental data taken from Ref. 23.
[b]Experimental data taken from Ref. 24.
[c]Experimental data taken from Ref. 41.

rule via the scaling factor λ_ε^{iR}. The results show that it is also possible to reproduce the binding affinity (Fig. S1).

In the alchemical transformation, we use a cycle that converts an arbitrary reference cation into ion i (with a specific value of the scaling factor λ_σ^{iR}). The binding affinity $\Delta G_b^i(\lambda_\sigma^{iR})$ is obtained from the free energy difference $\Delta\Delta G_b^i(\lambda_\sigma^{iR})$ of the transformation via

$$\Delta G_b^i(\lambda_\sigma^{iR}) = \Delta\Delta G_b^i(\lambda_\sigma^{iR}) - \Delta\Delta G_{solv}^i + \Delta G_b^{ref}, \quad (3)$$

where ΔG_b^{ref} is the binding affinity of the reference ion. $\Delta\Delta G_{solv}^i = \Delta G_{solv}^i - \Delta G_{solv}^{ref}$ is the difference of the solvation free energy of ion i and the reference ion. $\Delta\Delta G_b^i(\lambda_\sigma^{iR}) = \Delta G_b^i(\lambda_\sigma^{iR}) - \Delta G_b^{ref}$ is the difference of the binding affinity of ion i and the reference ion.

Without loss of generality, we choose Ca^{2+} with $\lambda_\sigma^{Ca^{2+}R} = 1$ as the reference, which yields $\Delta G_b^{ref} = -4.86\ k_BT$ and $\Delta G_{solv}^{ref} = -609.4\ k_BT$. The solvation free energy of Mg^{2+} and Ca^{2+} and the binding affinity of the reference ion were taken from our previous works.[12,20]

The alchemical transformation is particularly efficient to scan the λ_σ^{iR} parameter space since the terms $\Delta\Delta G_{solv}$ and ΔG_b^{ref} do not depend on λ_σ^{iR} and need to be calculated only once. Moreover, the term $\Delta\Delta G_b^i(\lambda_\sigma^{iR})$ is calculated by transforming a reference divalent cation, thereby avoiding the perturbation of the electrostatic part of the Hamiltonian. This leads to fast converging simulations and avoids the requirement of additional restraints or corrections.[20]

B. Performance of the optimized parameters for double-stranded DNA and the *add* A-riboswitch

To validate our parameters, three relevant nucleic acid systems were simulated. (i) A double-stranded DNA with three complete turns and 33 base pairs (bp), containing the same sequence as in Ref. 37, was simulated in the presence of 0.1 M $CaCl_2$. (ii) A 12 bp DNA identical to the x-ray structure crystallized in the presence of Ca^{2+} (pdb-id: 477d) was simulated with 0.06 M $CaCl_2$. The DNA systems were simulated for 2 μs using the parmbsc1[35] force field. (iii) A biologically relevant RNA system, the *add* A-riboswitch (pdb-id: 1y26), was simulated in the presence of neutralizing Mg^{2+} ions for 100 ns using the parmbsc0 + χ_{OL3} force field.[32–34] The simulation results were analyzed with x3DNA[38] and compared to the B-helix structure for the former system and to the x-ray structures for the latter cases.[39,40] Further details of the simulations and the analysis can be found in the supplementary material.

III. RESULTS

A. Optimization of ion–nucleic acid interactions based on ion binding affinities

The aim of our current work is to extend the applicability of bulk-optimized force field parameters[12] to quantitatively describe the interactions of Mg^{2+} and Ca^{2+} with nucleic acids. In general, the ionic atmosphere around nucleic acids consists of site-specific and diffusive ions. While the diffusive ions are well described by parameters that reproduce experimental bulk properties, the transferability of those parameters to describe site-specific ion–nucleic acid interactions is limited: Figs. 1(a) and 1(b) illustrate that the standard Lorentz rule significantly overestimates the binding affinity ΔG_b of Mg^{2+} and Ca^{2+} to the phosphate oxygen by 14 and 4 k_BT, respectively. In order to systematically adjust the ion–nucleic acid interactions without changing the bulk properties, we gradually modify the scaling parameter λ_σ^{iR} of the Lorentz rule [Eq. (2)] in a modest range ($0.9 < \lambda_\sigma^{iR} < 1.1$). Interestingly, slight changes in λ_σ^{iR} have a large effect on ΔG_b, which varies more than 35 k_BT. In both cases, small changes in λ_σ^{iR} and no changes in λ_ε^{iR} are sufficient to reproduce the experimental values (Tables I and II). Therefore, increasing the

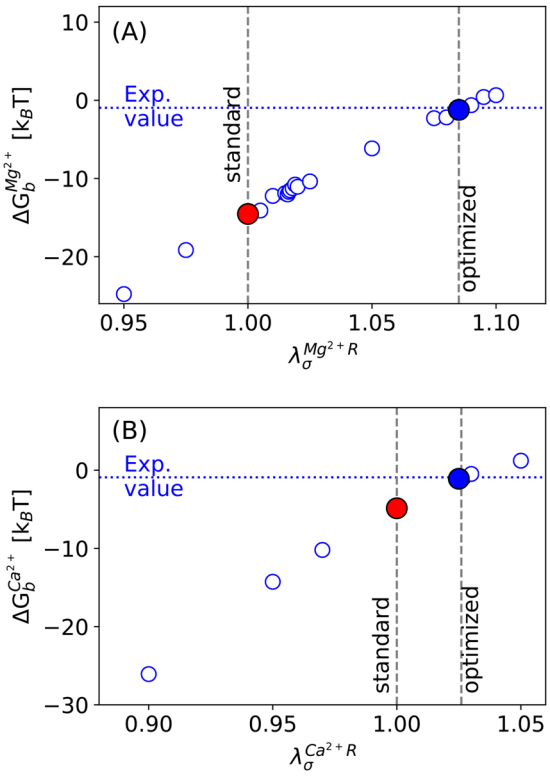

FIG. 1. Binding affinity ΔG_b^i (circles) to the phosphate oxygen as a function of the scaling factor λ_σ^{iR} [Eq. (3)] for Mg^{2+} (a) and Ca^{2+} (b). The horizontal dotted lines correspond to the experimental values.[23] Red and blue filled symbols indicate ΔG_b^i for the standard ($\lambda_\sigma^{iR} = 1$) and optimized (λ_σ^{iR*}) Lorentz combination rules, respectively.

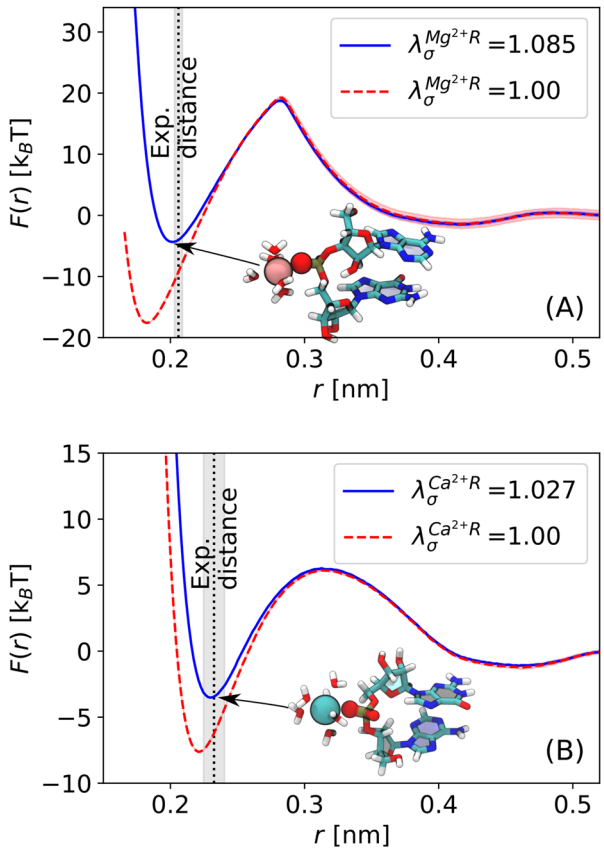

FIG. 2. Free energy profile as a function of the distance between the phosphate oxygen and Mg^{2+} (a) and Ca^{2+} (b). The snapshots show Mg^{2+} and Ca^{2+} in inner-sphere conformation. The vertical dotted lines indicate the experimental cation–phosphate oxygen distances R_b[24,41] listed in Table II.

effective diameter of the ion–oxygen pair by 8.5% and 2.7% allows us to exactly reproduce the experimental binding affinity.

Further insights on how a modification of the Lorentz rule affects ion binding are obtained from the free energy profiles as a function of the ion–phosphate oxygen distance [Figs. 2(a) and 2(b) and Fig. S2]. The free energy profiles have two stable states corresponding to Mg^{2+} or Ca^{2+} in inner-sphere or outer-sphere conformation. As expected, the depth of the first minimum that reflects the ion binding affinity is reduced for the optimized ($\lambda_\sigma^{iR*} > 1$) compared to the standard Lorentz rule ($\lambda_\sigma^{iR} = 1$). A further increase in λ_σ^{iR} destabilizes the inner-sphere contact pair (Fig. S2). Consequently, the binding free energy becomes positive, and it is no longer possible to match the experimental results. Moreover, for large values of λ_σ^{iR}, the system only adopts an outer-sphere binding geometry, which contradicts the results from crystal structures.[24,40] In addition, the free energy barrier of dissociation is reduced, indicating that the optimized parameters lead to faster dissociation kinetics. By contrast, the association barrier that is linked to the removal of a water molecule from the first hydration shell remains unaffected by the modifications as intended.

Interestingly, the position of the minimum is shifted to larger distances for the optimized Lorentz combination rule, leading to quantitative agreement with ion–oxygen distances R_b obtained from high-resolution crystal structures (Table II). This result is encouraging as the optimization of the binding affinities resulted in an unexpected improvement of structural properties of site-specific ions.

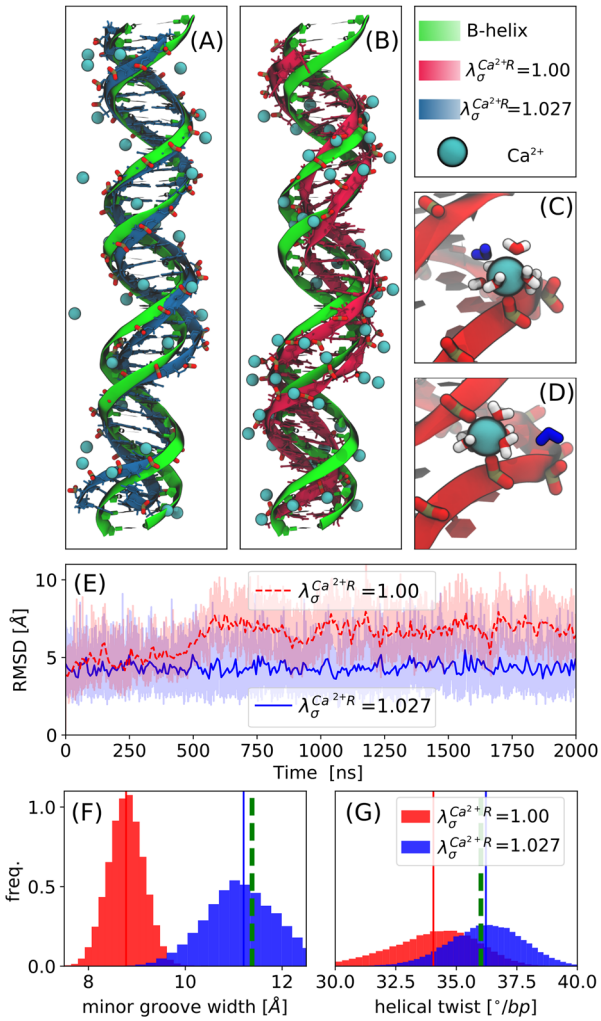

FIG. 3. Structure of a 33 bp DNA obtained from simulations. (a) and (b) Comparison of the averaged structure from the simulations with the optimized and standard Lorentz rule and an ideal B-helix (shown in green). (c) and (d) Formation of a Ca^{2+} bridge between the backbone strands via two inner-sphere contacts obtained with the standard Lorentz rule. The water molecule leaving the first hydration shell to facilitate the direct contact to the phosphate oxygen is shown in blue. (e) root-mean-squared deviation (RMSD) as a function of simulation time with respect to an ideal B-helix at every frame (transparent line) and averaged over a running window of 2000 frames (solid line). (f) and (g) Distributions and averages (vertical lines) of the minor groove width and the helical twist of DNA in comparison to the ideal B-helix (green dashed line).

TABLE III. Helical properties of DNA structures from experiments and simulations for standard ($\lambda_\sigma^{Ca^{2+}R}$ = 1.00) and optimized ($\lambda_\sigma^{Ca^{2+}R}$ = 1.027) Lorentz combination rules. Simulation values are the averages over the last 500 ns, and errors correspond to standard deviations.

		33 bp DNA			pdb-id: 477d DNA[a]		
Property	Unit	$\lambda_\sigma^{Ca^{2+}R}$ = 1.00	$\lambda_\sigma^{Ca^{2+}R}$ = 1.027	B-helix	$\lambda_\sigma^{Ca^{2+}R}$ = 1.00	$\lambda_\sigma^{Ca^{2+}R}$ = 1.027	X ray[a]
RMSD	Å	6.77 ± 0.09	4.49 ± 0.09	⋯	3.02 ± 0.03	2.58 ± 0.03	⋯
Minor groove width	Å	9.29 ± 0.35	11.53 ± 0.37	11.50	9.15 ± 0.56	10.93 ± 0.72	10.18
Major groove width	Å	22.34 ± 0.61	18.79 ± 0.46	17.62	20.62 ± 1.38	18.32 ± 1.01	17.58
Helical radius	Å	10.89 ± 0.22	10.84 ± 0.18	10.32	11.01 ± 0.46	10.78 ± 0.38	10.68
Helical twist	deg/bp	32.76 ± 0.80	35.34 ± 0.57	36.03	33.57 ± 2.10	36.30 ± 1.57	37.29
Helical rise	Å/bp	3.25 ± 0.06	3.26 ± 0.06	3.38	3.24 ± 0.11	3.31 ± 0.12	3.33

[a]X-ray structure taken from Ref. 39.

B. Performance of the optimized Ca^{2+} parameters for double-stranded DNA

The performance of the optimized Ca^{2+} parameters is investigated for two double-stranded DNA systems. The first system is a short 12 bp DNA with a sequence identical to a 1.7 Å x-ray crystal structure obtained in the presence of Ca^{2+}.[39] The second system is a longer 33 bp DNA with the same sequence as in Ref. 37. Here, no crystal structure in the presence of Ca^{2+} exists. However, experiments show that Ca^{2+} has a negligible effect on the bending of the helix, and an almost ideal B-helix form is expected.[39,42]

Figure 3 and Table III compare the equilibrium structures obtained from experiments and from simulations with the standard and optimized Lorentz rules for Ca^{2+}. The two DNA structures obtained with the standard combination rules deviate notably from the experimental results. The optimized combination rule provides significant improvement [Figs. 3(a) and 3(b)] and yields DNA structures close to the ideal B-helix [Fig. 3(e)] or the crystal structure (Fig. S3). In particular, the optimized Lorentz rule leads to a much closer agreement of the helical properties, including the minor groove width [Fig. 3(f)], the helical twist [Fig. 3(g)], the helical radius, and the rise (Table III).

Figures 3(a) and 3(b) and Fig. S3 reveal that the structural differences observed for the standard and optimized combination rules arise from the binding of Ca^{2+} to specific binding sites with different coordination modes. For the standard combination rule, a single Ca^{2+} ion can bind to multiple phosphate oxygens via inner-sphere contacts [Figs. 3(b) and 3(d)]. In particular, the Ca^{2+} ions bridge between the phosphate oxygens of opposite backbones, thereby shrinking the minor groove. Hereby, the bridging is formed in two steps. First, a partially dehydrated Ca^{2+} ion forms an inner-sphere contact with the phosphate oxygen from one backbone strand [Fig. 3(c)]. Subsequently, additional hydration water molecules are removed, and a second inner-sphere contact is formed with the second strand [Fig. 3(d)].

Overall, the bridging between the backbone strands observed with the standard combination rule leads to deviations from the ideal B-helix form or the experimental crystal structure where no bridging was observed. The bridging is a consequence of the overrated binding affinity obtained with the standard combination rules. For the optimized combination rule, in which the binding affinity is adjusted, no bridging is observed and the simulated DNA structures reproduce the experimental results much more closely.

C. Performance of the optimized parameters for the *add* A-riboswitch

Finally, we investigate the optimized Mg^{2+} parameters for the *add* A-riboswitch. This riboswitch is particularly suited for the

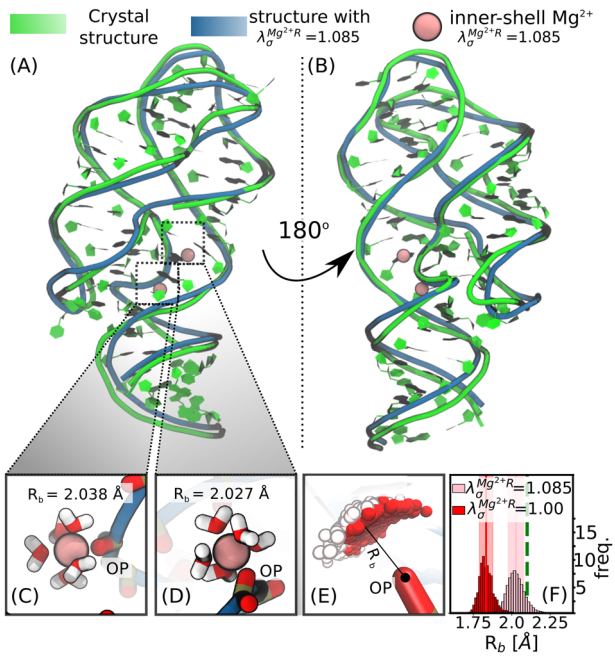

FIG. 4. *Add* A-riboswitch for the standard and optimized Lorentz rules for Mg^{2+}. (a) and (b) Crystal structure (green) and averaged structure obtained from simulations with the optimized Lorentz rule with an RMSD of 2.20 Å (blue). (c) and (d) Snapshots of the two inner-sphere Mg^{2+} ions, including the first ion hydration shell for the optimized Lorentz rule. (e) and (f) Distributions and average values (vertical lines) of the Mg^{2+}–phosphate oxygen distance R_b for the binding site shown in (d) for the standard ($\lambda_\sigma^{Mg^{2+}R}$ = 1.00) and optimized ($\lambda_\sigma^{Mg^{2+}R}$ = 1.085) Lorentz rules. The experimental value is shown as a green dashed line.

validation of the Mg^{2+} parameters since the experimental x-ray structure[40] includes two specifically bound Mg^{2+} ions. Initially, we investigate the stability of the RNA structure using the standard and optimized Lorentz rule for Mg^{2+} [Figs. 4(a) and 4(b)]. During the 100 ns simulation, the tertiary structure of the riboswitch remains stable and close to the experimental crystal structure with a root-mean-square deviation (RMSD) of 2.3 Å ($\lambda_\sigma^{iR} = 1$) and 2.2 Å ($\lambda_\sigma^{iR} = 1.085$). The two site-specific ions are in direct contact with the phosphate oxygens and remain in this inner-sphere conformation over the duration of the simulation. In addition, about 20 Mg^{2+} ions form transient outer-sphere contacts with phosphate oxygens, the nitrogen and oxygen atoms of the nucleobases, and the ribose oxygens (see the supplementary material), in agreement with recent observations.[24,25]

Figures 4(c) and 4(d) show Mg^{2+} at the two experimentally observed binding sites. The results reveal that the modification of the Lorentz rule has a significant effect on the distance between Mg^{2+} and the phosphate oxygen. For the standard rule, the distance at the first binding site is $R_b = 1.83 \pm 0.05$ Å, while the optimized rule yields a distance of $R_b = 2.03 \pm 0.05$ Å in close agreement with $R_b = 2.10$ Å in the x-ray structure [Figs. 4(e) and 4(f)]. The situation is similar for the second binding site. The standard combination rule yields a shorter distance of 1.83 ± 0.04 Å compared to 2.04 ± 0.06 Å observed for the optimized rule. Both values are significantly smaller compared to the 2.44 Å reported in the x-ray structure. However, note that the experimental value is located in the exclusion range and is therefore likely to be overrated. By contrast, the distances observed with the optimized Lorentz rule seem to provide a reliable estimate as judged by the assignment criterium of 2.06–2.08 Å.[24]

In summary, the standard and optimized combination rules for Mg^{2+} yield stable RNA structures. Moreover, the optimized Lorentz rule for ion–RNA interactions improves the structure of specifically bound ions and yields improved agreement with experimentally observed binding geometries.

IV. CONCLUSIONS

Mg^{2+} and Ca^{2+} are essential for the structure, folding, and function of nucleic acids. To correctly describe their interactions with DNA and RNA in biomolecular simulations, we have extended the applicability of bulk-optimized force field parameters[12] by including experimental binding affinities toward the phosphate oxygen.[23]

In agreement with previous results,[13,20] bulk-optimized force field parameters show too strong of an attraction between cations and specific ion binding sites. As illustrated for double-stranded DNA and the *add* A-riboswitch, this leads to deviations of simulated and experimental nucleic acid structures, for instance, due to unrealistic bridging effects between the backbone strands or very short distances to specific ion binding sites.

One possibility, to correct such shortcomings, is to use more complicated interaction potentials[13] to account for polarization and charge transfer effects that are likely the cause of the deviations.

Our approach shows that some of the effects of polarizability, which presumably cause the deviations from the standard combination rules, can also be taken into account via a scaling factor.[14] By modifying the Lorentz combination rule for the cation–nucleic acid interaction, the excessive binding of the metal cations can be corrected without changing the form of the commonly used 12-6 interaction potential. In particular, increasing the effective size of the cation–phosphate oxygen pair by a small amount via the scaling factor in the Lorentz combination rule allows us to exactly reproduce the experimental binding affinity toward the phosphate oxygen. The advancement of the optimization is clearly evident from the improved agreement between the simulated and experimental structures for double-stranded DNA.[42] Moreover, the optimization of the binding affinities resulted in an unexpected improvement of structural properties as shown, for instance, for the two specifically bound Mg^{2+} ions in the experimental structure of the *add* A-riboswitch.[40]

The advantage of this approach is that it leaves the ion–water and ion–ion interactions unchanged and can therefore be transferred easily to other ion binding sites on biomolecules. However, for other ion binding sites on RNA, in particular, the N7 and O6 atoms of the nucleobases, our previous work showed that the standard combination rules for Mg^{2+} and Ca^{2+} reproduce experimental binding affinities within error.[20] Still, more work and accurate experimental measurements are required to determine the scaling parameters for different ion binding sites on proteins or lipids. Nevertheless, including experimental binding affinities toward specific ion binding sites on biomolecules provides a promising perspective to develop a more accurate description of metal cations in biomolecular simulations.

SUPPLEMENTARY MATERIAL

Further details of the simulations and the analysis are provided in the supplementary material. The improved force field parameters are openly available at https://github.com/bio-phys/ff-Mg-Ca-NucleicAcids.

ACKNOWLEDGMENTS

This work was funded by the Emmy Noether Program of Deutsche Forschungsgemeinschaft (DFG, German Research Foundation) under Grant No. 315221747. The authors acknowledge GOETHE HLR for supercomputing access. N.S. thanks Roland R. Netz, Dominik Horinek, and Maria Fyta for inspiring and fruitful discussions.

DATA AVAILABILITY

The data that support the findings of this study are available from the corresponding author upon reasonable request.

REFERENCES

[1] S.-L. Yean, G. Wuenschell, J. Termini, and R.-J. Lin, Nature **408**, 881 (2000).
[2] S. Nakano, D. M. Chadalavada, and P. C. Bevilacqua, Science **287**, 1493 (2000).
[3] M. R. Stahley and S. A. Strobel, Science **309**, 1587 (2005).
[4] R. Strick, P. L. Strissel, K. Gavrilov, and R. Levi-Setti, J. Cell Biol. **155**, 899 (2001).
[5] N. Lehman and G. F. Joyce, Nature **361**, 182 (1993).
[6] D. N. Frank and N. R. Pace, Proc. Natl. Acad. Sci. U. S. A. **94**, 14355 (1997).
[7] P. Auffinger, N. Grover, and E. Westhof, Met. Ions Life Sci. **9**, 1 (2011).
[8] W. Zhou, R. Saran, and J. Liu, Chem. Rev. **117**, 8272 (2017).
[9] P. Li, B. P. Roberts, D. K. Chakravorty, and K. M. Merz, Jr., J. Chem. Theory Comput. **9**, 2733 (2013).

[10]M. T. Panteva, G. M. Giambaşu, and D. M. York, J. Comput. Chem. **36**, 970 (2015).
[11]S. Mamatkulov, M. Fyta, and R. R. Netz, J. Chem. Phys. **138**, 024505 (2013).
[12]S. Mamatkulov and N. Schwierz, J. Chem. Phys. **148**, 074504 (2018).
[13]M. T. Panteva, G. M. Giambaşu, and D. M. York, J. Phys. Chem. B **119**, 15460 (2015).
[14]M. Fyta and R. R. Netz, J. Chem. Phys. **136**, 124103 (2012).
[15]O. Allnér, L. Nilsson, and A. Villa, J. Chem. Theory Comput. **8**, 1493 (2012).
[16]N. Schwierz, J. Chem. Phys. **152**, 224106 (2020).
[17]M. Fyta, I. Kalcher, J. Dzubiella, L. Vrbka, and R. R. Netz, J. Chem. Phys. **132**, 024911 (2010).
[18]M. B. Gee, N. R. Cox, Y. Jiao, N. Bentenitis, S. Weerasinghe, and P. E. Smith, J. Chem. Theory Comput. **7**, 1369 (2011).
[19]S. Kashefolgheta and A. Vila Verde, Phys. Chem. Chem. Phys. **19**, 20593 (2017).
[20]S. Cruz-León and N. Schwierz, Langmuir **36**, 5979 (2020).
[21]S. R. van Lin, K. K. Grotz, I. Siretanu, N. Schwierz, and F. Mugele, Langmuir **35**, 5737 (2019).
[22]J. Yoo and A. Aksimentiev, J. Phys. Chem. Lett. **3**, 45 (2012).
[23]R. K. O. Sigel and H. Sigel, Acc. Chem. Res. **43**, 974 (2010).
[24]F. Leonarski, L. D'Ascenzo, and P. Auffinger, Nucleic Acids Res. **45**, 987 (2017).
[25]F. Leonarski, L. D'Ascenzo, and P. Auffinger, RNA **25**, 173 (2019).
[26]S. Weerasinghe and P. E. Smith, J. Chem. Phys. **119**, 11342 (2003).
[27]B. Hess and N. F. A. van der Vegt, Proc. Natl. Acad. Sci. U. S. A. **106**, 13296 (2009).
[28]H. A. Lorentz, Ann. Phys. **248**, 127 (1881).
[29]D. Berthelot, C. R. Acad. Sci. **126**, 1703 (1898).
[30]I. V. Leontyev and A. A. Stuchebrukhov, J. Chem. Phys. **141**, 014103 (2014).
[31]I. M. Zeron, J. L. F. Abascal, and C. Vega, J. Chem. Phys. **151**, 134504 (2019).
[32]W. D. Cornell, P. Cieplak, C. I. Bayly, I. R. Gould, K. M. Merz, D. M. Ferguson, D. C. Spellmeyer, T. Fox, J. W. Caldwell, and P. A. Kollman, J. Am. Chem. Soc. **117**, 5179 (1995).
[33]A. Pérez, I. Marchán, D. Svozil, J. Sponer, T. E. Cheatham, C. A. Laughton, and M. Orozco, Biophys. J. **92**, 3817 (2007).
[34]M. Zgarbová, M. Otyepka, J. Šponer, A. Mládek, P. Banáš, T. E. Cheatham, and P. Jurečka, J. Chem. Theory Comput. **7**, 2886 (2011).
[35]I. Ivani, P. D. Dans, A. Noy, A. Pérez, I. Faustino, A. Hospital, J. Walther, P. Andrio, R. Goñi, A. Balaceanu *et al.*, Nat. Methods **13**, 55 (2016).
[36]W. L. Jorgensen, J. Chandrasekhar, J. D. Madura, R. W. Impey, and M. L. Klein, J. Chem. Phys. **79**, 926 (1983).
[37]F. Kriegel, C. Matek, T. Dršata, K. Kulenkampff, S. Tschirpke, M. Zacharias, F. Lankaš, and J. Lipfert, Nucleic Acids Res. **46**, 7998 (2018).
[38]X.-J. Lu and W. K. Olson, Nat. Protoc. **3**, 1213 (2008).
[39]G. Minasov, V. Tereshko, and M. Egli, J. Mol. Biol. **291**, 83 (1999).
[40]A. Serganov, Y.-R. Yuan, O. Pikovskaya, A. Polonskaia, L. Malinina, A. T. Phan, C. Hobartner, R. Micura, R. R. Breaker, and D. J. Patel, Chem. Biol. **11**, 1729 (2004).
[41]S. K. Kolev, P. S. Petkov, M. A. Rangelov, D. V. Trifonov, T. I. Milenov, and G. N. Vayssilov, Metallomics **10**, 659 (2018).
[42]T. K. Chiu and R. E. Dickerson, J. Mol. Biol. **301**, 915 (2000).